Analysis and Characterization of Multilayered Reflector Antennas: Rain/Snow Accumulation and Deployable Membrane

Hung-Piu Ip and Yahya Rahmat-Samii, *Fellow, IEEE*

***Abstract*—There are important engineering issues in designing reflector antennas that cannot be addressed by simply assuming a perfect electric conductor (PEC) reflector surface. For example, coatings may exist on antenna surfaces for protection, rain or snow can accumulate on outdoor reflectors, and the deployable mesh or inflatable membrane antennas usually do not have solid PEC reflector surfaces. Physical optics (PO) analysis remains the most popular method of reflector analysis owing to its inherent simplicity, accuracy, and efficiency. The conventional PO analysis is performed under the assumption of perfectly conducting reflector surface. To generalize the PO analysis to arbitrary reflector surfaces, a modified PO analysis is presented. Under the assumptions of locally planar reflector surface and locally planewave characteristic of the waves incident upon the reflector surface, the reflection and transmission coefficients at every point of the reflector surface are determined by the transmission-line analogy to the multilayered surface structure. The modified PO currents, taking into account by the finite transmissions of the incident waves, are derived from the reflection and transmission coefficients. Applications on the analyses of the rain and snow accumulation effects on the direct-broadcast TV antennas and the effects of finite thickness and finite conductivity of the metal coating on a 15-m inflatable antenna are described and results are presented.**

***Index Terms*—DBS antennas, inflatable membrane, lossy material, physical optics, rain/snow, reflector antennas.**

I. Introduction

In order to design and correctly predict the performance of a reflector antenna, different analysis and synthesis techniques have been developed [1]–[3]. Among these techniques, physical optics (PO) analysis remains one of the most popular for the calculation of radiation patterns. PO analysis usually assumes the reflector surface under analysis to be perfect electric conductor (PEC). The assumption of PEC reflector surfaces is generally true as most reflector surfaces are merely metal sheets that are much thicker than the skin depths of the metals and with very high conductivities. There are, however, many practical situations in which the assumption of total reflection does not necessarily hold. The frequency-selective surface (FSS) reflector antennas are manufactured from surface materials which allow waves to pass through. To provide a means of protection, the metal reflector surface(s) of a reflector antenna may be coated with a thin epoxy layer. In case of bad weather, it is a common experience that receptions from outdoor reflectors will be degraded by the rain or snow accumulation on the reflector surfaces. An inflatable reflector antenna is realized by coating a thin metal layer on a dielectric membrane. If the thickness of the metal layer is much greater than the skin depth of the metal, total reflection is expected. If the order of magnitude of the metal thickness is comparable to the skin depth, total reflection is not guaranteed. For a mesh-deployable antenna, the reflector surface is usually perforated metal surface or empty spaces with some interwoven metal wires running in between. In any of the examples described above, the assumption of PEC for the reflector surfaces is definitely inappropiate. In order to analyze these situations, PO analysis must be modified in such a way for which nontotal reflection, in general, can be correctly accounted.

Mesh-deployable and FSS reflectors have been topics of research interest for decades. Publications including the theoretical analysis and experiment application can be found [4]–[7]. Inflatable reflector antenna has also attracted a lot of attention since two to three decades ago [4], [8], [9]. Though researches on the electrical aspects of inflatable antennas are abundant, most of the analyses still assumed the reflector surface to be perfectly conducting. Some experiments have been conducted in relation to the effect of dielectric coating, rain precipitation, and snow accretion on the performance of reflector antennas [10], [11], but not much work has been done on the general analysis and simulation of the situations. To the best of the author's knowledge, no rigorous analysis on the effect of finite thickness and finite conductivity of metal coatings on inflatable antennas or the effects of coating, partial depletion of coating, rain and snow accumulations on the performance of the 18-in direct-broadcast TV antenna has been found in the literature.

This work extends the conventional PO analysis of reflector antennas to an analysis capable of handling general reflector surfaces. Section II explains the methodology of the solution for the modified PO analysis. Derivation of the modified PO currents on arbitrary multilayered planar surfaces follows in Section III. Based on the currents obtained, the formulation of the modified PO currents on general reflector surfaces is then presented in Section IV. The approach is in close resemblance to the analyses of mesh-deployable antennas [5] and FSS antennas [7]. A computer program is developed for the PO analysis of reflector antennas with arbitrary surfaces. Applica-

Manuscript received October 7, 1997; revised June 9, 1998. This work was supported in part by JPL under Contract Number 960591.

The authors are with the Department of Electrical Engineering, University of California, Los Angeles, CA 90095 USA.

Publisher Item Identifier S 0018-926X(98)08876-0.

0018–926X/98$10.00 © 1998 IEEE

tions of the modified PO analysis, including the effects of rain precipitation and snow accumulation on the direct-broadcast TV antenna and the effects of membrane's finite thickness and finite conductivity on inflatable antennas, are illustrated in Section V. A conclusion of the major achievements of this work is summarized in Section VI. Finally, a method of solution to the general plane-waves propagation through isotropic and homogeneous multilayered media is presented in Appendix A for completion.

II. Solution Methodology

The PO analysis is based on the theory of PO equivalence, which can be considered as a limiting case of the more general equivalence theorem [12, pp. 329–334]. The equivalence theorem states that the E and H fields at any observation point outside the source(s) (the antenna in this case) can be obtained upon the calculation of the surface currents on a surface completely enclosing the source(s). The currents include both the electric $\vec{J}_s(\vec{r}')$ and magnetic $\vec{M}_s(\vec{r}')$ currents and are merely the result of the total electric and magnetic fields on the surface

$$\vec{M}_s(\vec{r}') = -\hat{n} \times [\vec{E}^i(\vec{r}') + \vec{E}^r(\vec{r}')]|_{S^f} \tag{1}$$

$$\vec{J}_s(\vec{r}') = \hat{n} \times [\vec{H}^i(\vec{r}') + \vec{H}^r(\vec{r}')]|_{S^f} \tag{2}$$

$$\vec{M}_s(\vec{r}') = -\hat{n} \times \vec{E}^t(\vec{r}')|_{S^b} \tag{3}$$

$$\vec{J}_s(\vec{r}') = \hat{n} \times \vec{H}^t(\vec{r}')|_{S^b} \tag{4}$$

where $\vec{r}'$ and $\hat{n}$ are the position vector and outward unit normal of a source point on the reflector surface, $\vec{E}^i(\vec{r}')/\vec{H}^i(\vec{r}')$, $\vec{E}^r(\vec{r}')/\vec{H}^r(\vec{r}')$ and $\vec{E}^t(\vec{r}')/\vec{H}^t(\vec{r}')$ are the incident, reflected, and transmitted electric/magnetic field intensities on the reflector surface S^f and S^b are the front (illuminated) and back (shadow) surfaces of the reflector, respectively.

Upon the calculation of the surface currents, the resultant E and H fields at any observation point can then be expressed as [12, pp. 279, 286]

$$\vec{E}(\vec{r}) = -\frac{j}{\omega\epsilon}\int_S [(\vec{J}_s(\vec{r}')\cdot\nabla)\nabla + k^2\vec{J}_s(\vec{r}')]\frac{e^{-jkR}}{4\pi R}\,dS' - \int_S \vec{M}_s(\vec{r}')\times\nabla\left(\frac{e^{-jkR}}{4\pi R}\right)dS' \tag{5}$$

$$\vec{H}(\vec{r}) = -\frac{j}{\omega\mu}\int_S [(\vec{M}_s(\vec{r}')\cdot\nabla)\nabla + k^2\vec{M}_s(\vec{r}')]\frac{e^{-jkR}}{4\pi R}\,dS' + \int_S \vec{J}_s(\vec{r}')\times\nabla\left(\frac{e^{-jkR}}{4\pi R}\right)dS' \tag{6}$$

where ω is the angular frequency, ϵ and μ are the permittivity and permeability of free-space, k is the free-space wavenumber, R is the distance from the observation point to the source point, S is the reflector surface, $j = \sqrt{-1}$, and the time convention $e^{j\omega t}$ is adopted.

As shown in Fig. 1, owing to the continuity of the electric field at any material interface, if the reflecting surface is thin or the reflection coefficient Γ is close to -1, the tangential component of the transmitted E field $(\vec{E}^t)$ on the back of the reflector is close to the sum of the tangential components of the incident and reflected E fields $(\vec{E}^i + \vec{E}^r)$ and, thus, the magnetic current on the back side of the reflector $(\vec{M}_s^b)$ is almost the same as the one on the front $(\vec{M}_s^f)$ and the net magnetic current is close to zero (i.e., $\vec{M}_s^f + \vec{M}_s^b \sim 0$). As a result, $\vec{M}_s$ is negligible and, thus, only $\vec{J}_s$ is necessary for the computation of the antenna pattern. PO analysis usually assume the reflector surface under analysis to be PEC and so total reflection on the reflector surface is a consequence, i.e., $\Gamma = -1$. Under this assumption, only $\vec{J}_s(\vec{r}')$ exists and the the PO surface current $\vec{J}_s(\vec{r}')$ on the reflector surface can be written as [3]

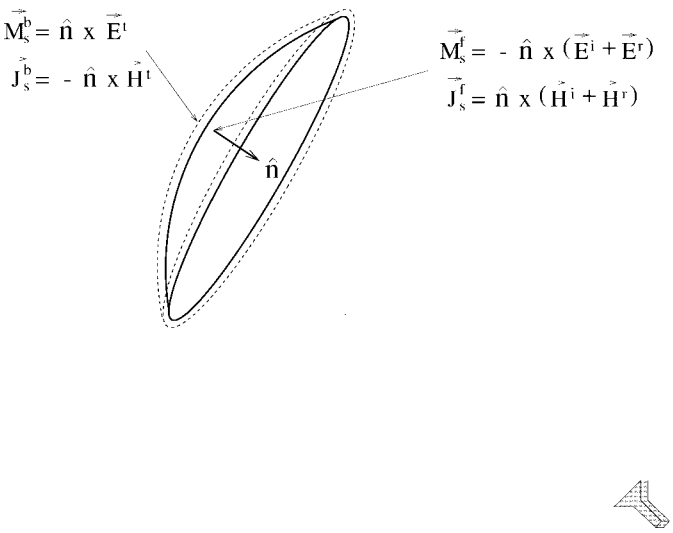

Fig. 1. Application of the equivalence theorem on the reflector surface for current calculation.

$$\vec{J}_s(\vec{r}') = 2\hat{n} \times \vec{H}^i(\vec{r}'). \tag{7}$$

Upon the calculation of $\vec{J}_s(\vec{r}')$, the $\vec{E}(\vec{r})$ and $\vec{H}(\vec{r})$ fields at any observation point P with position vector $\vec{r}$ can be calculated from (5) and (6) by simply excluding the magnetic current $\vec{M}_s(\vec{r}')$.

Since the assumption of total reflection does not hold for a non-PEC reflector surface, both the electric $(\vec{J}_s)$ and magnetic $(\vec{M}_s)$ currents exist on the reflector surface and the computation of the far-field radiation pattern of a reflector with non-PEC surface structure requires the calculation of both currents.

The calculation of $\vec{J}_s$ and $\vec{M}_s$ requires the knowledge of the reflection and transmission coefficients (Γ and τ) at every point on the reflector surface (see Sections III and IV for details). Obtaining the reflection and transmission coefficients is, in general, not an easy task owing to the finiteness in dimensions and nonplanarity in curvatures of most reflector surfaces and the nonplanar wave nature of the electromagnetic waves incident upon the reflector surfaces.

Fortunately, two approximations allow the problem to be greatly simplified. In order to calculate the E and H fields numerically, the reflector surface has to be subdivided into a number of subsurfaces. If the subdivision is sufficiently small, the reflector subsurfaces can be approximated by locally planar subsurfaces. The reflector is usually assumed to be large in terms of wavelength and the feeds are in the far-field zones

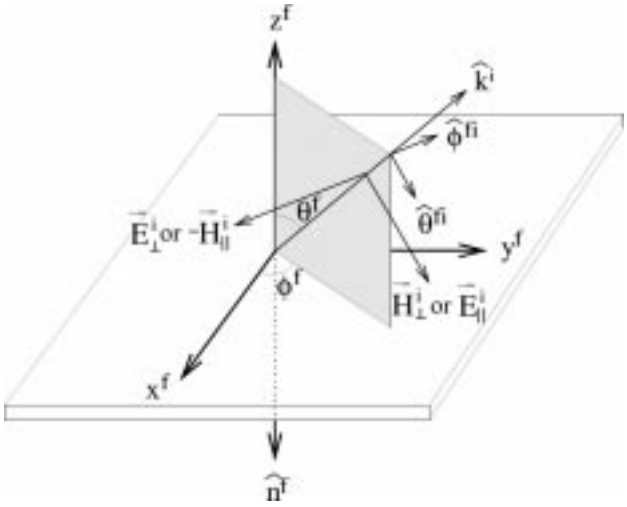

Fig. 2. Plane waves incidence on multilayered planar surface: perpendicular polarization ($\vec{E}^i_\perp$, $\vec{H}^i_\perp$), and parallel polarization ($-\vec{H}^i_\parallel$, $\vec{E}^i_\parallel$).

with respect to the antenna surface so that the waves impinging upon the reflector surface are virtually locally plane waves. Based on these approximations, namely, the locally planar approximation of the reflector surfaces and the locally planar approximation of the incident waves, the current distribution within each of the subsurfaces is essentially constant and the integration of the current distribution then essentially becomes a summation of the currents on each of the subsurfaces. This suggests that the reflection and transmission coefficients can be deduced from the solution to the canonical problem of plane waves propagation through infinitely two-dimensional (2-D) planar multilayered structures. Hence, the key point of the analysis is to compute the total currents on each of the planar approximation to the subsurfaces, which in turn requires the knowledge of the reflection and transmission coefficients at that subsurface. The methods of solution of computing the reflection and transmission coefficients of plane waves propagation through 2-D, infinitely planar multilayered media can then be implemented into the evaluation of the modified PO currents. One method of solution is the application of the transmission line theory, as summarized in Appendix A.

III. Modified PO Current on Planar Multilayered Structure

To construct the modified PO currents on planar multilayered surface illuminated by plane waves of oblique incidence, a local coordinate system is first defined at the interface. The waves are decomposed into the perpendicular and parallel polarizations (as illustrated in Fig. 2) where $(x^f,\ y^f,\ z^f)$, $(r^f,\ \theta^f,\ \phi^f)$ are the local Cartesian and spherical coordinate systems at the front surface, $\hat{k}^i$ is the unit vector in the incidence direction, ϕ^{fi} and θ^{fi} are the the ϕ and θ coordinates of the incident waves with respect to the local spherical coordinate system, $\vec{E}^i(\vec{r}^f)$ and $\vec{H}^i(\vec{r}^f)$ are the incident E and H fields at the observation point $\vec{r}^f$

$$\hat{\phi}^{fi} = -\hat{x}^f \sin\phi^{fi} + \hat{y}^f \cos\phi^{fi} \tag{8}$$

and

$$\hat{\theta}^{fi} = (\hat{x}^f \cos\phi^{fi} + \hat{y}^f \sin\phi^{fi})\cos\theta^{fi} - \hat{z}^f \sin\theta^{fi}. \tag{9}$$

The incident E and H fields impinging upon the interface, i.e., $z^f = 0$, can then be written as

$$\vec{E}^i(\vec{r}^f) = \{-\hat{\phi}^{fi}E^i_\perp(\vec{r}^f) + \hat{\theta}^{fi}E^i_\parallel(\vec{r}^f)\}e^{-j\vec{k}^i\cdot\vec{r}^f} \tag{10}$$

$$\vec{H}^i(\vec{r}^f) = \frac{1}{\eta}\{\hat{\theta}^{fi}E^i_\perp(\vec{r}^f) + \hat{\phi}^{fi}E^i_\parallel(\vec{r}^f)\}e^{-j\vec{k}^i\cdot\vec{r}^f} \tag{11}$$

where $k = \frac{2\pi}{\lambda}$, $E^i_\perp(\vec{r}^f)$ and $E^i_\parallel(\vec{r}^f)$ are the perpendicular and parallel polarizations of the incident E field, respectively, and

$$\vec{k}^i = k_o[(\hat{x}^f \cos\phi^{fi} + \hat{y}^f \sin\phi^{fi})\sin\theta^{fi} + \hat{z}^f \cos\theta^{fi}]. \tag{12}$$

The transmitted E and H fields exiting the structure, i.e., $z^f = d$ where d is the total thickness of the multilayered structure, are given by

$$\vec{E}^t(\vec{r}^b) = \{-\hat{\phi}^{fi}\tau_\perp E^i_\perp(\vec{r}^f) + \hat{\theta}^{fi}\tau_\parallel E^i_\parallel(\vec{r}^f)\}e^{-j\vec{k}^i\cdot\vec{r}^b} \tag{13}$$

$$\vec{H}^t(\vec{r}^b) = \frac{1}{\eta}\{\hat{\theta}^{fi}\tau_\perp E^i_\perp(\vec{r}^f) + \hat{\phi}^{fi}\tau_\parallel E^i_\parallel(\vec{r}^f)\}e^{-j\vec{k}^i\cdot\vec{r}^b} \tag{14}$$

where $\tau_\perp$ and $\tau_\parallel$ are the transmission coefficients of the perpendicular and parallel polarizations of the transmitted E field at the back surface, respectively, and

$$\vec{r}^b = \vec{r}^f + d\hat{z}^f \tag{15}$$

is the position vector of the point of transmission on the back surface.

Similarly, the reflected E and H fields can be expressed by

$$\vec{E}^r(\vec{r}^f) = \{-\hat{\phi}^{fr}\Gamma_\perp E^i_\perp(\vec{r}^f) + \hat{\theta}^{fr}\Gamma_\parallel E^i_\parallel(\vec{r}^f)\}e^{-j\vec{k}^r\cdot\vec{r}^f} \tag{16}$$

$$\vec{H}^r(\vec{r}^f) = \frac{1}{\eta}\{\hat{\theta}^{fr}\Gamma_\perp E^i_\perp(\vec{r}^f) + \hat{\phi}^{fr}\Gamma_\parallel E^i_\parallel(\vec{r}^f)\}e^{-j\vec{k}^r\cdot\vec{r}^f} \tag{17}$$

where $\Gamma_\perp$ and $\Gamma_\parallel$ are the reflection coefficients of the perpendicular and parallel polarizations of the E field at the front surface, respectively

$$\begin{aligned}\vec{k}^r &= \vec{k}^i - 2(\vec{k}^i\cdot\hat{z}^f)\hat{z}^f \\ &= k_o[(\hat{x}^f\cos\phi^{fi} + \hat{y}^f\sin\phi^{fi})\sin\theta^{fi} - \hat{z}^f\cos\theta^{fi}]\end{aligned} \tag{18}$$

$$\hat{\phi}^{fr} = -\hat{x}^f\sin\phi^{fi} + \hat{y}^f\cos\phi^{fi} \tag{19}$$

and

$$\hat{\theta}^{fr} = -(\hat{x}^f\cos\phi^{fi} + \hat{y}^f\sin\phi^{fi})\cos\theta^{fi} - \hat{z}^f\sin\theta^{fi}. \tag{20}$$

The transmission and reflection coefficients for the perpendicular and parallel polarizations at the front interface can be obtained from (78), (79), (88), and (89) in Appendix A and are repeated here as follows:

$$\Gamma_\perp, \Gamma_\parallel = \frac{A + \frac{B}{Z_t} - Z_i\left(C + \frac{D}{Z_t}\right)}{A + \frac{B}{Z_t} + Z_i\left(C + \frac{D}{Z_t}\right)} \tag{21}$$

$$\tau_\perp, \tau_\parallel = \frac{2}{A + \frac{B}{Z_t} + Z_i\left(C + \frac{D}{Z_t}\right)} \tag{22}$$

where

$$Z_k = \begin{cases}\eta_k \sec\theta_k & \text{for perpendicular polarization} \\ \eta_k \cos\theta_k & \text{for parallel polarization}\end{cases} \tag{23}$$

η_k and γ_k are the intrinsic impedance and propagation constant of the kth medium, respectively, $k = i, 1, 2, \cdots, n, t$, where i and t are the indexes of the semi-infinite incident and transmitted media, respectively, θ_i is the real angle of incidence at the semi-infinite incident medium, θ_m and θ_t are the complex angles of incidence and transmission at the mth medium and the semi-infinite transmitted medium respectively, d_m is the thickness of the mth medium

$$\begin{bmatrix} A & B \\ C & D \end{bmatrix} = \begin{bmatrix} A_1 & B_1 \\ C_1 & D_1 \end{bmatrix} \begin{bmatrix} A_2 & B_2 \\ C_2 & D_2 \end{bmatrix} \cdots \begin{bmatrix} A_n & B_n \\ C_n & D_n \end{bmatrix} \tag{24}$$

$$A_m = \cosh(\gamma_m \cos\theta_m d_m) \tag{25}$$
$$B_m = \sinh(\gamma_m \cos\theta_m d_m) Z_m \tag{26}$$
$$C_m = \frac{\sinh(\gamma_m \cos\theta_m d_m)}{Z_m} \tag{27}$$
$$D_m = \cosh(\gamma_m \cos\theta_m d_m) \tag{28}$$

for $m = 1, 2, \cdots, n$.

The total electric and magnetic currents ($\vec{J}_s^f(\vec{r}^f)$ and $\vec{M}_s^f(\vec{r}^f)$) on the front interface of the multilayered surface structure are contributed from the incident and the reflected fields and are given by

$$\vec{J}_s^f(\vec{r}^f) = \hat{n}^f \times [\vec{H}^i(\vec{r}^f) + \vec{H}^r(\vec{r}^f)]|_{\vec{r}^f \in S^f} \tag{29}$$
$$= -\hat{z}^f \times [\vec{H}^i(\vec{r}^f) + \vec{H}^r(\vec{r}^f)]|_{\vec{r}^f \in S^f} \tag{30}$$
$$\vec{M}_s^f(\vec{r}^f) = -\hat{n}^f \times [\vec{E}^i(\vec{r}^f) + \vec{E}^r(\vec{r}^f)]|_{\vec{r}^f \in S^f} \tag{31}$$
$$= \hat{z}^f \times [\vec{E}^i(\vec{r}^f) + \vec{E}^r(\vec{r}^f)]|_{\vec{r}^f \in S^f} \tag{32}$$

where S^f represents the loci of points on the front interface and $\hat{n}^f = -\hat{z}^f$ is the unit outward normal on the front interface at $\vec{r}^f$.

The total electric and magnetic currents ($\vec{J}_s^b(\vec{r}^b)$ and $\vec{M}_s^b(\vec{r}^b)$) on the back interface of the multilayered surface structure are contributed from the transmitted fields only and are expressed by

$$\vec{J}_s^b(\vec{r}^b) = \hat{n}^b \times \vec{H}^t(\vec{r}^b)|_{\vec{r}^b \in S^b} \tag{33}$$
$$= \hat{z}^f \times \vec{H}^t(\vec{r}^b)|_{\vec{r}^b \in S^b} \tag{34}$$
$$\vec{M}_s^b(\vec{r}^b) = -\hat{n}^b \times \vec{E}^t(\vec{r}^b)|_{\vec{r}^b \in S^b} \tag{35}$$
$$= -\hat{z}^f \times \vec{E}^t(\vec{r}^b)|_{\vec{r}^b \in S^b} \tag{36}$$

where S^b represents the loci of points on the back interface and $\hat{n}^b = -\hat{n}^f = \hat{z}^f$ is the unit outward normal on the back interface at $\vec{r}^b$.

Thus, the total modified PO currents consist of both the electric and magnetic currents, where the values on the front and back sides are given by (29)–(36).

Since no assumption has been made on the materials composing the multilayered planar surface, the analysis discussed in this section is generic and can be applied to any infinitely planar multilayered surface structure provided the parameters of the material for each layer can somehow be obtained.

If the total thickness of the layers are negligibly small compared to wavelength, $S^f \simeq S^b$ and the transmission and reflection coefficients at the interface are, from the continuity of electric field across the boundary, simply related as

$$1 + \Gamma_\perp = \tau_\perp \tag{37}$$
$$1 - \Gamma_\parallel = \tau_\parallel. \tag{38}$$

In that case, the total magnetic current vanishes since the electric fields on both sides of the multilayered structure must be equal (i.e., continuity of electric field across boundary) and the total current simply reduces to the electric current only. The total current $\vec{J}_s(\vec{r}^f)$ at the interface is given by

$$\vec{J}_s(\vec{r}^f) = \hat{n}^f \times [\vec{H}^i(\vec{r}^f) + \vec{H}^r(\vec{r}^f) - \vec{H}^t(\vec{r}^f)]. \tag{39}$$

Substituting (11), (14), and (17) into (39), the current can be written as

$$\vec{J}_s(\vec{r}^f) = \vec{J}^{\mathrm{PO}}(\vec{r}^f) - \vec{J}^{ft}(\vec{r}^f) \tag{40}$$

where

$$\vec{J}^{\mathrm{PO}}(\vec{r}^f) = 2\hat{n}^f \times \vec{H}^i(\vec{r}^f)$$

$$\begin{aligned} \vec{J}^{ft}(\vec{r}^f) &= \frac{2}{\eta}\hat{n}^f \times \{\hat{\theta}^{fi}\tau_\perp \vec{E}_\perp^i(\vec{r}^f) + \hat{\phi}^{fi}\tau_\parallel \vec{E}_\parallel^i(\vec{r}^f)\} \\ &= \frac{2}{\eta}\hat{n}^f \times \{\hat{x}^f[\cos\theta^{fi}\sin\phi^{fi}\tau_\perp \vec{E}_\perp^i(\vec{r}^f) \\ &\quad + \cos\phi^{fi}\tau_\parallel \vec{E}_\parallel^i(\vec{r}^f)] \\ &\quad + \hat{y}^f[-\cos\theta^{fi}\cos\phi^{fi}\tau_\perp \vec{E}_\perp^i(\vec{r}^f) \\ &\quad + \sin\phi^{fi}\tau_\parallel \vec{E}_\parallel^i(\vec{r}^f)]\}. \end{aligned} \tag{41}$$

The current $\vec{J}_s(\vec{r}^f)$ given by (40) is the modified PO current deduced in [5] and [7] for the analysis of thin-mesh deployable and frequency-selective surface reflector antennas. Note that the modified current in this case is essentially the conventional PO current $\vec{J}^{\mathrm{PO}}(\vec{r}^f)$ less the induced current $\vec{J}^{ft}(\vec{r}^f)$ due to finite transmission of the plane waves through the multilayered media.

If the layers are replaced by a perfect electric conductor, $\vec{J}^{ft}(\vec{r}^f)$ becomes zero owing to zero transmission and the analysis is further simplified to the conventional PO analysis.

IV. Modified PO Current on Layered Reflector Surface

As discussed in Section I, a reflector surface is divided into subsurfaces for numerical computation and each subsurface is approximated by a tangent plane about some point P within the subsurface. The modified PO currents are evaluated from (29) to (36), as detailed in Section III. Upon the evaluation of the modified PO currents, the E and H fields at any observation point $\vec{r}$ can be calculated from (5) and (6).

In order to calculate the currents, the local coordinate systems at every tangent plane must be defined. The $\hat{z}^f$ direction is defined as $\hat{z}^f = -\hat{n}^f$, where $\hat{n}^f$ is the inward normal at P. Assuming the reflector surface is described by an analytical equation $z_P = f(x_P, y_P)$, where (x_P, y_P, z_P) are the Cartesian coordinates of P with respect to the main

reflector coordinate system, then the unit normal $\hat{n}^f$ at any point P on the reflector surface can be obtained from

$$\hat{n}^f = \frac{1}{\sqrt{f_x^2 + f_y^2 + 1}}(-\hat{x}f_x - \hat{y}f_y + \hat{z}) \tag{42}$$

where

$$f_x = \left.\frac{\partial f}{\partial x}\right|_P, \quad f_y = \left.\frac{\partial f}{\partial y}\right|_P.$$

The $\hat{x}^f$ and $\hat{y}^f$ directions can be specified by any two orthogonal unit vectors lying on the tangent plane. The orientations of $\hat{x}^f$ and $\hat{y}^f$ are absolutely immaterial to the final result. One way of defining the vectors is as follows:

$$\hat{x}^f = \hat{x} \times \hat{z}^f \tag{43}$$
$$\hat{y}^f = \hat{z}^f \times \hat{x}^f \tag{44}$$

if $\hat{x} \neq \hat{z}^f$

$$\hat{x}^f = \hat{y} \times \hat{z}^f \tag{45}$$
$$\hat{y}^f = \hat{z}^f \times \hat{x}^f \tag{46}$$

if $\hat{x} = \hat{z}^f$.

To obtain the perpendicular and parallel directions for the decomposition of the E field into the two polarizations, the direction of incidence $\hat{k}^i$ must first be calculated. The direction of incidence is the direction from the phase center of the feed to the point P where the approximating tangent plane to the subsurface is defined. $\hat{k}^i$ can be evaluated by joining the phase center of the feed to the point P. If the center of the feed and the point P are denoted by (x_F, y_F, z_F) and (x_P, y_P, z_P) with respect to the main reflector coordinate system then

$$\hat{k}^i = \frac{\hat{x}(x_P - x_F) + \hat{y}(y_P - y_F) + \hat{z}(z_P - z_F)}{\sqrt{(x_P - x_F)^2 + (y_P - y_F)^2 + (z_P - z_F)^2}}. \tag{47}$$

Thus

$$\hat{k}_\perp = (\hat{z}^f \times \hat{k}^i) \times \hat{k}^i \tag{48}$$
$$\hat{k}_\parallel = \hat{z}^f \times \hat{k}^i \tag{49}$$

where $\hat{k}_\perp$ and $\hat{k}_\parallel$ are the unit vectors in the perpendicular and parallel directions, respectively.

The total modified PO current on each of the subsurface is the sum of all the modified PO currents originated from all the feeds in the system, as shown in Fig. 3. Since the transmission coefficients $\tau_\parallel$ and $\tau_\perp$, as well as the reflection coefficients $\Gamma_\parallel$ and $\Gamma_\perp$, are different for different polarizations of oblique incidences (Appendix A), the modified PO currents generated by each of the nth feed is a function of the angle of incidence θ_n^i. The angle θ_n^i is defined as the angle between $\hat{k}_n^i$ and $\hat{z}^f$, where $\hat{k}_n^i$ is the unit wave vector of the incident waves from the nth feed to the point P where the approximating tangent plane to the subsurface is resided and $\hat{z}^f$ is the outward unit normal to the approximating tangent plane at P. $\hat{z}^f = -\hat{n}^f$ can be calculated from (42) and $\hat{k}_n^i$ can be evaluated from (47) by replacing (x_F, y_F, z_F) by (x_{Fn}, y_{Fn}, z_{Fn}) and $\hat{k}^i$ by $\hat{k}_n^i$.

So far, all the currents are expressed with respect to the local coordinate systems of the subsurfaces. To calculate the resultant E and H fields, a single-reference coordinate system must be defined and all the quantities expressed in the local coordinate systems have to be transformed into the reference coordinate system. One way of doing this is to use the main reflector coordinate system as the reference. All the quantities expressed in the local coordinate systems can be transformed into the main reflector coordinate system through the Eulerian transformation [13].

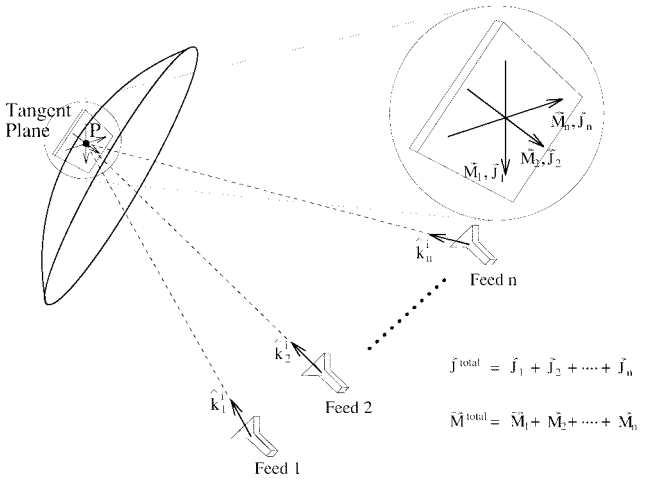

Fig. 3. Calculation of the total modified PO currents on a subsurface.

The method of analysis remains the same as that of the conventional PO analysis except that the conventional PO electric current has to be replaced by the modified PO electric and magnetic currents. Considering the currents on the front and the back sides of the reflector surface, (5) and (6) can be rewritten as

$$\begin{aligned}\vec{E}(\vec{r}) = &-\frac{j}{\omega\epsilon}\int_{S^f}[(\vec{J}_s(\vec{r}^{\,f})\cdot\nabla)\nabla + k^2\vec{J}_s(\vec{r}^{\,f})]\frac{e^{-jkR^f}}{4\pi R^f}\,dS' \\ &-\frac{j}{\omega\epsilon}\int_{S^b}[(\vec{J}_s(\vec{r}^{\,b})\cdot\nabla)\nabla + k^2\vec{J}_s(\vec{r}^{\,b})]\frac{e^{-jkR^b}}{4\pi R^b}\,dS' \\ &-\int_{S^f}\vec{M}_s(\vec{r}^{\,f})\times\nabla\left(\frac{e^{-jkR^f}}{4\pi R^f}\right)dS' \\ &-\int_{S^b}\vec{M}_s(\vec{r}^{\,b})\times\nabla\left(\frac{e^{-jkR^b}}{4\pi R^b}\right)dS'\end{aligned} \tag{50}$$

$$\begin{aligned}\vec{H}(\vec{r}) = &-\frac{j}{\omega\mu}\int_{S^f}[(\vec{M}_s(\vec{r}^{\,f})\cdot\nabla)\nabla + k^2\vec{M}_s(\vec{r}^{\,f})]\frac{e^{-jkR^f}}{4\pi R^f}\,dS' \\ &-\frac{j}{\omega\mu}\int_{S^b}[(\vec{M}_s(\vec{r}^{\,b})\cdot\nabla)\nabla + k^2\vec{M}_s(\vec{r}^{\,b})]\frac{e^{-jkR^b}}{4\pi R^b}\,dS' \\ &+\int_{S^f}\vec{J}_s(\vec{r}^{\,f})\times\nabla\left(\frac{e^{-jkR^f}}{4\pi R^f}\right)dS' \\ &+\int_{S^b}\vec{J}_s(\vec{r}^{\,b})\times\nabla\left(\frac{e^{-jkR^b}}{4\pi R^b}\right)dS'.\end{aligned} \tag{51}$$

For a far-field application

$$S^f \simeq S^b \tag{52}$$
$$R^f \simeq R^b \simeq r \tag{53}$$

$$e^{-jkR^f} = e^{-j\hat{k}^i\cdot(\vec{r}-\vec{r}^f)} = e^{-j\hat{k}^i\cdot\vec{r}} \cdot e^{j\hat{k}^i\cdot\vec{r}^f} \tag{54}$$

$$e^{-jkR^b} = e^{-j\hat{k}^i\cdot(\vec{r}-\vec{r}^b)} = e^{-jkR^f} \cdot e^{jkd\cos(\theta^{fi})} \tag{55}$$

where R^f and R^b are the distances between the source points $\vec{r}^f$ on the front interface and $\vec{r}^b$ on the back interface to the observation point $\vec{r}$, respectively.

Thus, (50) and (51) can be rewritten as

$$\vec{E}(\vec{r}) \simeq j\omega\frac{e^{-jkr}}{4\pi r}\Bigg\{-\mu\int_{S^f}\big[\vec{J}_s^f(\vec{r}^f) + \vec{J}_s^b(\vec{r}^b)e^{jkd\cos(\theta^{fi})}\big]e^{-jk\hat{r}\cdot\vec{r}^f}\,dS' + k\hat{r} \times \int_{S^f}\big[\vec{M}_s^f(\vec{r}^f) + \vec{M}_s^b(\vec{r}^b)e^{jkd\cos(\theta^{fi})}\big] \cdot e^{-jk\hat{r}\cdot\vec{r}^f}\,dS'\Bigg\} \tag{56}$$

$$\vec{H}(\vec{r}) \simeq j\omega\frac{e^{-jkr}}{4\pi r}\Bigg\{-\epsilon\int_{S^f}\big[\vec{M}_s^f(\vec{r}^f) + \vec{M}_s^b(\vec{r}^b)e^{jkd\cos(\theta^{fi})}\big]e^{-jk\hat{r}\cdot\vec{r}^f}\,dS' - k\hat{r} \times \int_{S^f}\big[\vec{J}_s^f(\vec{r}^f) + \vec{J}_s^b(\vec{r}^b)e^{jkd\cos(\theta^{fi})}\big]e^{-jk\hat{r}\cdot\vec{r}^f}\,dS'\Bigg\}. \tag{57}$$

V. Application

Numerous source codes for the analysis of general reflector antennas based on the PO current approach are readily obtainable. Most of these source codes, however, do not include the non-PEC effect of the reflector surface. The modified PO currents on a subsurface generated by a single feed or an array of feeds can be calculated from (1) to (4), where both the electric and magnetic currents are included. In these equations, the reflection and transmission coefficients for both the perpendicular and parallel components are required. A subroutine capable of evaluating these coefficients is written. To develop a program for the analysis of reflector antennas with arbitrary surface structure, the reflector source codes can be modified by including the subroutine at the stage of the modified PO currents calculation. With the modified PO current being calculated, the modified PO analysis discussed in Section IV can be performed.

A computer program is developed for the modified PO analysis of general reflector systems. Applications to the analysis of reflectors with various surface structures are given in the following sections. Although the program is capable of analyzing non-PEC dual and multiple reflector systems, the emphasis of this work is primarily focused on single reflector antennas.

It is noted in Section II that if the reflector surface is thin or the conductivity is high, the contribution from the magnetic current is small and can thus be neglected. The exclusion of the magnetic current simplifies the computer program and reduces the time for calculation; a fact that might have to be considered when efficiency and simplicity are more important than accuracy.

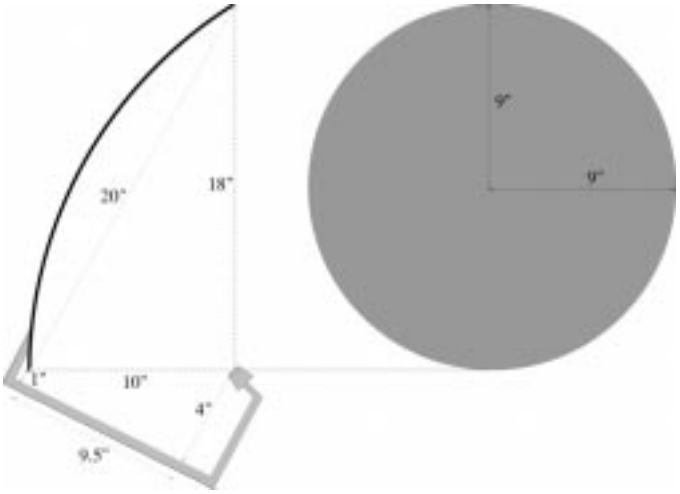

Fig. 4. Typical dimensions of an 18-in direct-broadcast TV antenna.

A. Direct-Broadcast TV Antenna: Effects of Rain and Snow on the Antenna Performance

Since the direct-broadcast TV antennas must be installed outdoor for satellite reception, it is obvious that they are subjected to outdoor weather conditions. Analyses of the direct-broadcast TV antennas under outdoor circumstances are, therefore, highly desirable. Yet, not many works can be found on this aspect. This subsection provides some results for the effects of rain and snow precipitations on the performance of the direct-broadcast TV antennas.

Typical dimensions for an 18-in direct-broadcast TV antenna is shown in Fig. 4. The antenna is an offset parabolic reflector that has a circular projected aperture of diameter 18 in. A cosine-Q feed of $Q_x = Q_y = 4.0$ and edge tapers at about 10 dB is simulated to provide the maximum possible antenna gain. The signals received from the satellites have a frequency range from 12.2 to 12.7 GHz and a cross-polarization level better than 27 dB down from the copolarization [14]. The center frequency at 12.5 GHz is assumed for all the calculations. The goal is to determine the antenna far-field radiation patterns at the two principal cuts ($\phi = 0°$ and $\phi = 90°$) and then to analyze the performance. In practice, left circular polarization (LCP) and right circular polarization (RCP) may be used in different areas of coverage and, thus, the analysis should be performed with both circular polarizations. Throughout this section, however, only LCP is assumed. The case of RCP will be the same as the LCP except that the radiation patterns for the RCP in $\phi = 90°$ plane are the mirror images of the LCP ones about the $\theta = 0°$ axis. A beam squint [15] of about 0.32° in the $\phi = 0°$ plane is observed for the LCP configuration. This agrees with the theoretical value

$$\theta_s = \arcsin\left\{\frac{\sin(\theta_o)}{2fk}\right\} = 0.322° \tag{58}$$

where θ_s and θ_o are the squint angle and the angle between the z axis of the main reflector coordinate system and the boresight direction of the feed respectively and f is the focal length.

Effect of Rain Precipitation: To protect against corrosion and solar heating, some reflector antennas are covered with a

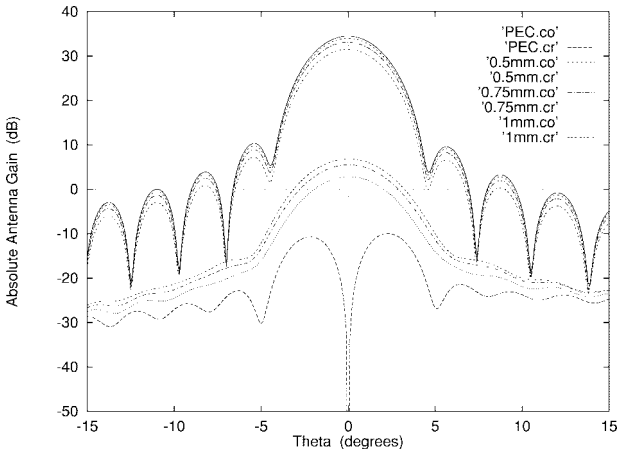

Fig. 5. Far-field radiation patterns in the $\phi = 0^\circ$ plane of the direct-broadcast TV reflector antenna with rain precipitation. The thickness of the water film is fixed at $t_w = 0.5$ mm. The thickness of the dielectric coating varies from $t_d = 0.5$ to 1.00 mm. The "PEC" cases refers to the ones without water film and dielectric coating.

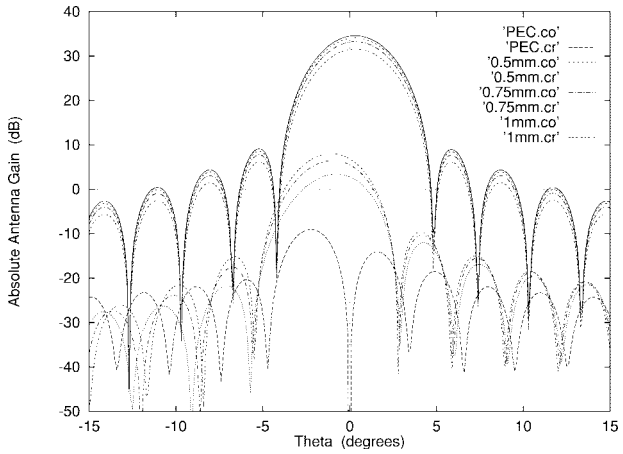

Fig. 6. Far-field radiation patterns in the $\phi = 90^\circ$ plane of the direct-broadcast TV reflector antenna with rain precipitation. The thickness of the water film is fixed at $t_w = 0.5$ mm. The thickness of the dielectric coating varies from $t_d = 0.5$ to 1.00 mm. The "PEC" cases refers to the ones without water film and dielectric coating.

layer of uniform, homogeneous, dielectric coating. Typical examples of dielectric coatings includes fiberglass (e.g., epoxide) and painting. Coatings are usually assumed to be uniform and thin, as suggested in [16], and, therefore, supposed to have no significant impact on the overall performance of the reflectors. Thus, reflector surfaces are simply assumed to be PEC for most of the reflector analyses. This is true if the coatings are thin compared to wavelengths and the reflectors are operating under good weather conditions. In case of rainy condition, as shown later in this section, the presence of the dielectric coatings may have disastrous effects on the performance of the antennas.

To demonstrate the effect of rain precipitation on the direct-broadcast TV antenna, a water film of thickness $t_w = 0.1$ mm and dielectric constant $\epsilon_w = 55.4 - j35.45$, as suggested in [10] and [17], is placed on top of a dielectric coating of relative dielectric constant $\epsilon_d = 4.5 - j0.009$ and thicknesses varying from $t_d = 0.5$ mm to 1.00 mm. The values of the dielectric constants are calculated at 12.5 GHz. The results are illustrated in Figs. 5 and 6.

For comparsion, the gain of an uncoated antenna with water film of thicknesses ranging from $t_w = 0.05$ to 0.1 mm is also studied and the results show that for the range of thicknesses concerned, the gain of the uncoated antenna is pratically not degraded at all (less than 0.05 dB at worst). This is true since the range of thicknesses of the water film is small compared to wavelength. In the presence of the dielectric coating, however, the loss due to the water film is strongly magnified. From Figs. 5 and 6, it is obvious that degradations in antenna performance under the influence of rain precipitation depends very much on the thickness of the dielectric coating. The cross polarization increases as t_d increases. More importantly, rapid loss in antenna gain is observed when the thickness of the coating increased from 0.50 to 1.00 mm. For a thickness of $t_d = 1.0$ mm, the decrease in gain is about 3 dB, which represents half of the total incident energy. If the thickness is changed to $t_d = \frac{\lambda_d}{2} = 5.657$ mm, however, the loss in gain is expected to be minimized. To the best of the author's knowledge, none of the commercially available direct-broadcast TV antennas have a half-wavelength coating. Also, bear in mind that so far, all the computations assume the operating frequency to be the center frequency at 12.5 GHz. In practice, the antennas receive a band of frequencies from 12.2 to 12.7 GHz and, thus, the choice of $t_d = 5.657$ mm minimizes the loss at the center frequency, but not at the other frequencies. For this reason, it may be advantageous to make the dielectric coating as thin as possible.

Effect of Snow Accretion: Since the direct-broadcast TV antenna must be installed outdoors, it is subjected to snow accretion in snowy areas. To align the antenna boresight direction with the line-of-sight of the satellite to the antenna, the antenna is usually tilted. Depending on the angle of elevation of the antenna, different amounts of snow will accumulate on the reflector surface. It is well known that the antenna performance is greatly degraded by the accreted snow on the reflector surface. Some experimental works [11] have been found in relation to the snow accretion on a communication antenna system, but none, to the best of the author's knowledge, is related to the 18-in direct-broadcast TV antenna.

The dielectric constant of the snow at 12.5 GHz is taken to be $\epsilon_s = 3.3 - j1.65$, according to [12]. The thickness of the snow is chosen to be $t_s = 3$ cm according to [11]. The snow accretion is simulated by a layer of uniform dielectric with the above dielectric constant and thickness and completely covering the part of the reflector surface extending from the bottom to a certain height h above that bottom in the projected aperture of the reflector (Fig. 7).

To investigate the effect of different heights of snow accretion on the performance of the direct-broadcast TV antenna, the thicknesses of the dielectric coating t_d and snow t_s are kept constant. Figs. 8 and 9 show the results for $t_s = 3$ cm and $t_d = 1.00$ mm. It must be emphasized that snow accretion on a reflector surface is highly nonuniform in thickness and the dielectric constant varies slightly across the entire surface. The choices of uniform thickness and constant relative permittivity

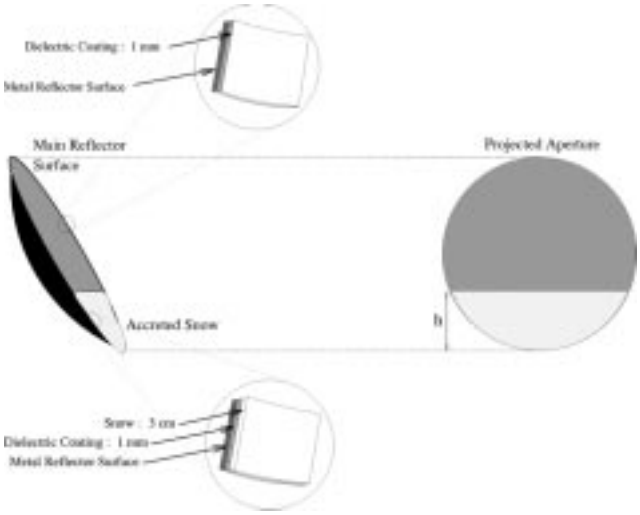

Fig. 7. Configuration of the snow accretion on the direct-broadcast TV antenna. The reflector surface is covered by a layer of snow of height h from the bottom of the projected aperture of the antenna.

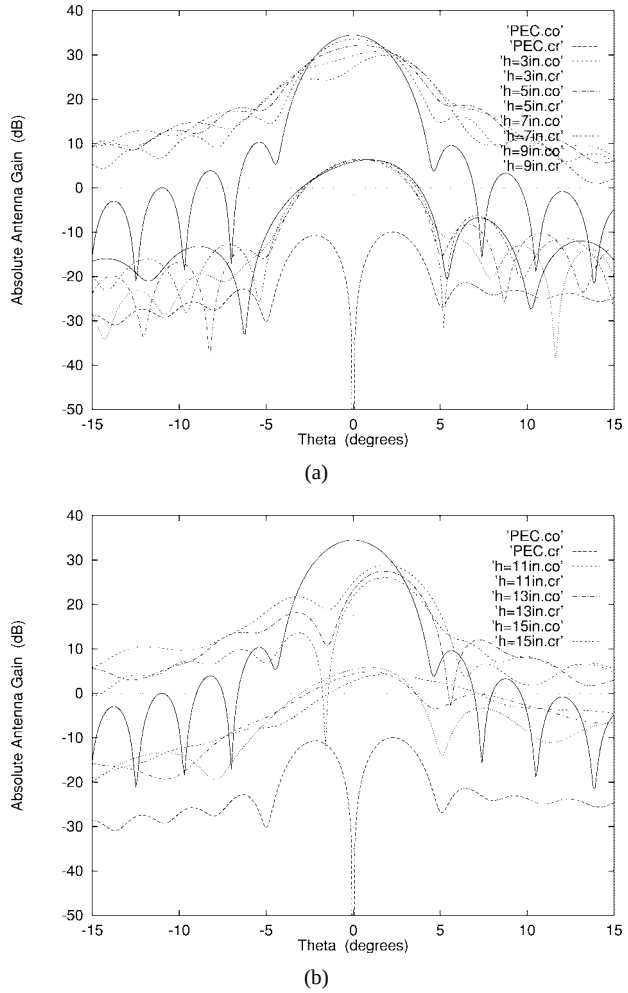

Fig. 8. Far-field radiation patterns in the $\phi = 0^\circ$ plane of the direct-broadcast TV reflector antenna with different heights of the snow accretion. The thickness of the accreted snow is fixed at $t_s = 3$ cm. The thickness of the dielectric coating is fixed at $t_d = 1.00$ mm. The heights of snow varies from $h = 3$ to 9 in. The "PEC" cases refers to the ones without accreted snow and dielectric coating.

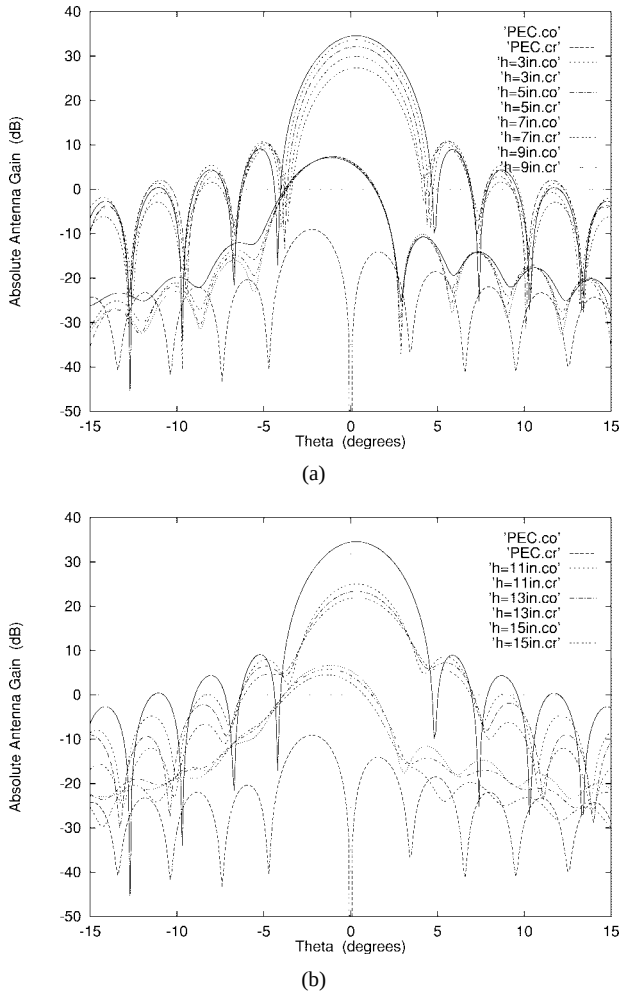

Fig. 9. Far-field radiation patterns in the $\phi = 90^\circ$ plane of the direct-broadcast TV reflector antenna with different heights of the snow accretion. The thickness of the accreted snow is fixed at $t_s = 3$ cm. The thickness of the dielectric coating is fixed at $t_d = 1.00$ mm. The heights of snow varies from $h = 3$ to 9 in. The "PEC" cases refers to the ones without accreted snow and dielectric coating.

in the above configuration reveal that the model of snow given above is not equivalent to the realistic problem. Moreover, the Jacobians for the projected aperture integration are assumed to remain unchanged throughout the analysis. Such assumption is good if the thickness is small compared to wavelength, but discrepancy is expected if the thickness is large. The analysis, however, does not intend to be exact, but instead offers some insights into the ways the antenna performance are changed. Though not exactly the same as the realistic case, it provides some good estimates of the magnitude and trend of degradations of the overall antenna performance and is thus deemed to be useful in this sense.

According to the results, the degradations of the antenna is highly dependent on the amount of snow accreted. In general, dramatic decrease in antenna gain and increase in sidelobe levels, rapid filling of nulls, gradual increase in cross polarization, and gradual splitting and shifting of the mainbeam in the $\phi = 0^\circ$ plane occur as the height of the snow increases. For $h = 5$ in (4 in below the center), the loss in gain is already about 3 dB.

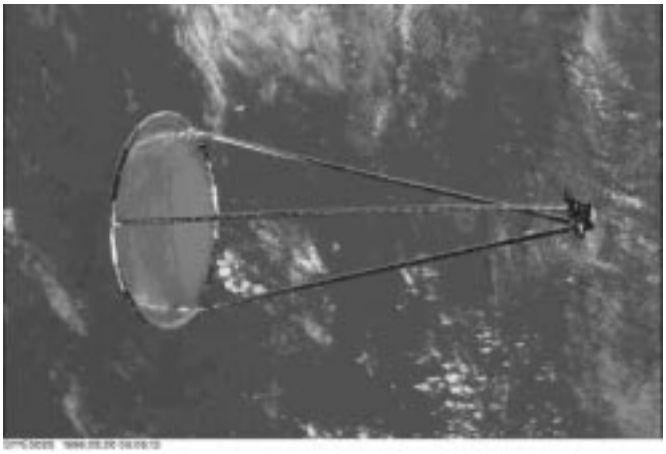

Fig. 10. An inflatable antenna in space (source: NASA Shuttle Web: Electronics still camera photos at website address http://shuttle.nasa.gov/sts-77/images/esc/day2.html).

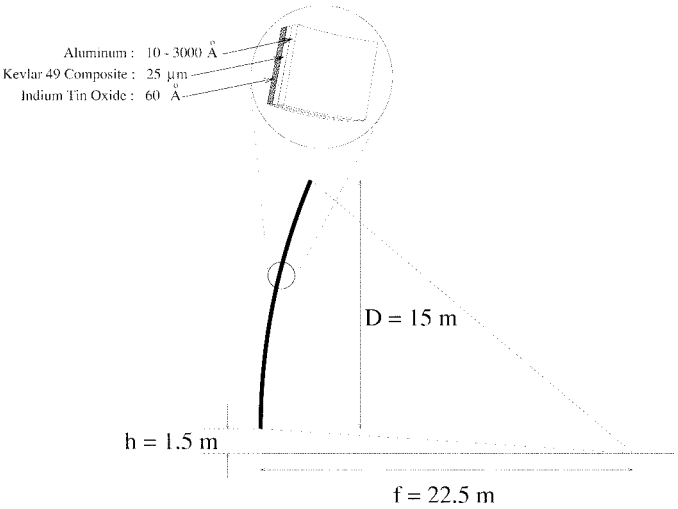

Fig. 11. Configuration of the 15-m offset-parabolic inflatable antenna.

B. Inflatable Antenna: Effects of Membrane's Finite Thickness and Finite Conductivity on the Antenna Performance

Inflatable antennas (Fig. 10) are built of a hydrocarbon dielectric layer (e.g., Kevlar, Mylar, Kapton) with a metal coating (e.g., aluminum, silver, gold) on the reflective or illuminated side and another protective layer (e.g., silicon oxide, indium tin oxide) on the radome or unilluminated side. The conductivity of the metal is assumed to be very large (of the order of 10^7 S/m) and the thickness of the dielectric is assumed to be large compared to the skin depth of the metal at that frequency. Hence, total reflection is resulted. However, the thicker the metal coating, the higher the cost of production and, thus, it is desirable to know the limit of thickness, which results in acceptable degradations in the antenna performance. It has been suggested in [18] that if the thickness of the metal coating is within the range of 100 to 3000 Å, then the loss in antenna gain due to the finite thickness or conductivity of the metal is virtually negligible. However, no published results are given to substantiate this observation. In [19], an aluminum coating of thickness 60 Å is proposed for an inflatable antenna system, but no consideration is given to the possible degradations in the antenna performance with that specified thickness. For a high-performance satellite antenna system, the loss of gain by 0.1 dB is already significant. It is thus desirable to have quantitative results showing the exact degradations of the antenna performance for different thicknesses of metal. Moreover, it is stated [8] that the conductivity of the metal layer may degrade during manufacturing and packaging. To analyze the effect of degradation in conductivity on the performance of the antenna, metal layers of different conductivities must be used.

This subsection gives some results of the effects of finite thickness and finite conductivity on the performance of an inflatable reflector. The configuration is a 15-m reflector antenna operating at 1.4 GHz (L-band), typical for mobile communications. The antenna system, depicted in Fig. 11, consists of a 15-m offset-parabolic reflector surface with offset height $h = 1.5$ m and focal length $f = 22.5$ m. The large focal length $(f/D = 1.5)$ is used for possible wide-angle scanning applications. The feed is modeled by a cosine Q feed of approximately 10.5-dB edge taper and the reflector is left-circularly polarized. The reflector surface is assumed to be composed of Kevlar 49 composite of thickness 25×10^{-6} m and dielectric constant $\epsilon_d = 3.45 - j0.051\,75$ (according to [20]), a metal coating of aluminum of conductivity $\sigma = 3.96 \times 10^7$ S/m (according to [12]) on the reflective side and an indium tin oxide coating of thickness 60 Å (according to [19]) and dielectric $\text{constant} = 4.0 - j0.013$ (according to [21]) on the radome side.

Effect of Finite Thickness: To study the effect of finite thickness on the antenna performance, different thicknesses of aluminum within the range of 3000 to 10 Å are used. The results are depicted in Figs. 12 and 13. From the results, we observe that except for the loss in gain, the copolarization characteristics are virtually unaffected. No beam-broadening, sidelobe level increase or null-filling is observed. The sidelobe levels actually decreased insignificantly as compared to the case of PEC surface. The loss in gain is negligible if the thickness t_m is greater than several hundred Å. This is interesting since a thickness of several hundred Å is much smaller than the skin depth δ of aluminum ($\sim$20 000 Å at 1.4 GHz) and yet finite transmission is virtually nonexistent. For a thickness of 100 Å, the loss in gain is about 0.1 dB, which may be important for some application. The maximum reduction in gain is about 1.1 dB and occurs when $t_m = 10$ Å. The cross polarization is slightly degraded as the thickness t_m is decreased from 3000 Å to 10 Å. Cross-polarization degradations include the increase in maximum level, increase in sidelobe level, and null filling, especially around the center. The increase in the maximum cross polarization is at worst about 10 dB and occurs at $t_m = 10$ Å. The maximum cross-polarization level, however, is at worst about 51 dB down from the copolarization for all thicknesses for this circular-polarization operation.

Effect of Finite Conductivity: To analyze the effect of the degradation in conductivity on the performance of the antenna, metal layers of conductivities $\sigma = 10^6$, 10^5, and 10^4 S/m and thickness t_d fixed at 1000 Å are simulated. The results are depicted in Figs. 14 and 15. From the results, we observe that

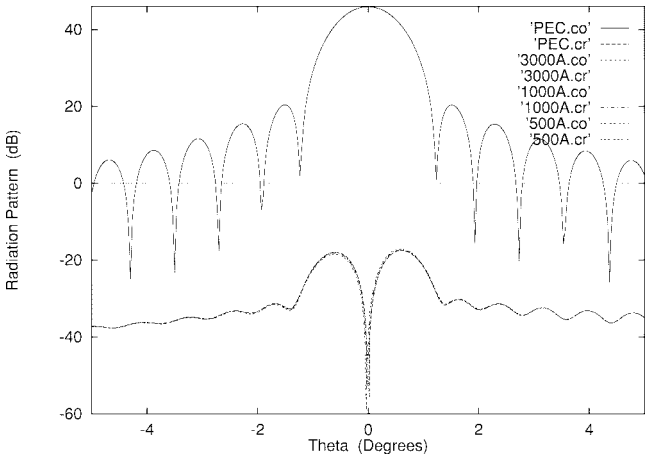

(a)

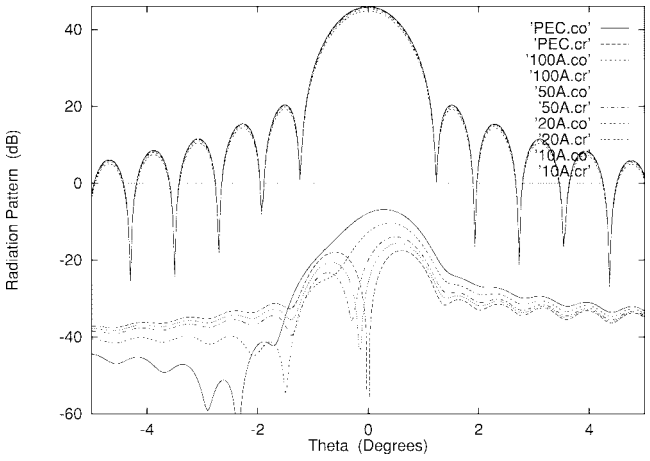

(b)

Fig. 12. Far-field radiation patterns in the $\phi = 0^\circ$ plane of the inflatable reflector antenna with different thicknesses of aluminum. The antenna is a 15-m offset-parabolic reflector fabricated of kevlar backed by aluminum on the reflective surface and indium tin oxide on the radome surface. The frequency is 1.4 GHz (L-band).

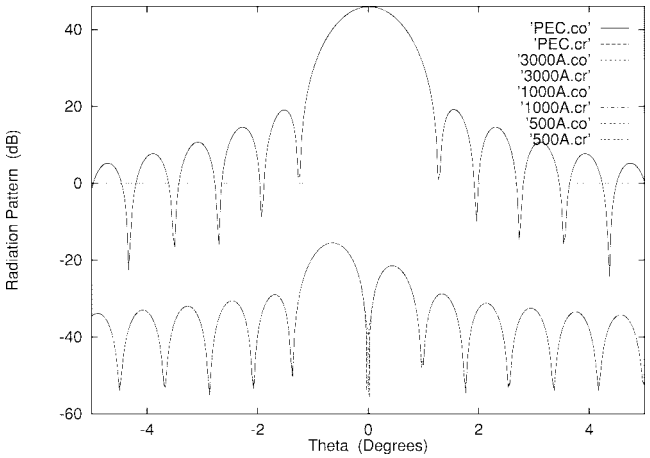

(a)

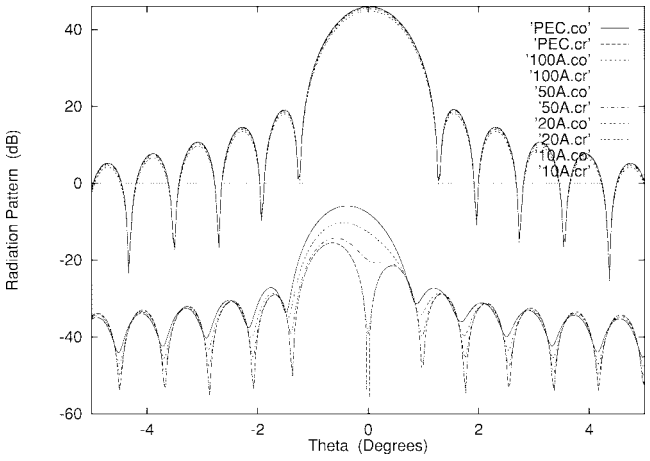

(b)

Fig. 13. Far-field radiation patterns in the $\phi = 90^\circ$ plane of the inflatable reflector antenna with different thicknesses of aluminum. The antenna is a 15-m offset-parabolic reflector fabricated of kevlar backed by aluminum on the reflective surface and indium tin oxide on the radome surface. The frequency is 1.4 GHz (L-band).

the loss in conductivity is disastrous. For the same thickness $t_m = 1000$ Å, the loss in gain for a conductivity of 10^6 S/m (σ of mercury, $\delta \sim 130\,000$ Å) is about 0.45 dB. For a conductivity of 10^5 S/m (σ of graphite, $\delta \sim 430\,000$ Å) the loss is about 3.7 dB—more than half of the total energy. The copolarization decreases rapidly as σ decreases.

VI. Conclusion

In this paper, a method of analysis for the reflector antennas with nonperfectly conducting surface structures was developed, and the analyses and characterizations of such reflector systems were presented. The proposed approach was a modification of the conventional PO analysis that was capable of analyzing general reflector surface structures including nonperfectly conducting ones. The reflection and transmission of plane waves through multilayered media with the aids of the transmission line analogy was studied. A computer subroutine was developed for this purpose. The derivation of the modified PO analysis was elaborated. Applications addressing the effects of rain precipitation and snow accre-

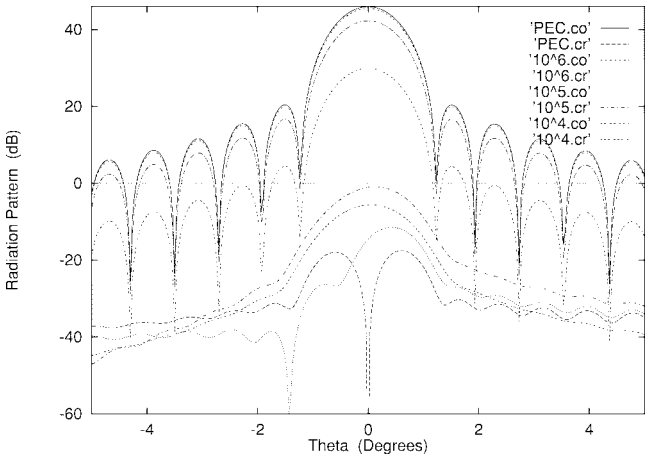

Fig. 14. Far-field radiation patterns in the $\phi = 0^\circ$ plane of the inflatable reflector antenna with different conductivities (S/m) of metal. The antenna is a 15-m offset-parabolic reflector fabricated of mylar backed by aluminum on the reflective surface and indium tin oxide on the radome surface. The frequency is 1.4 GHz (L-band).

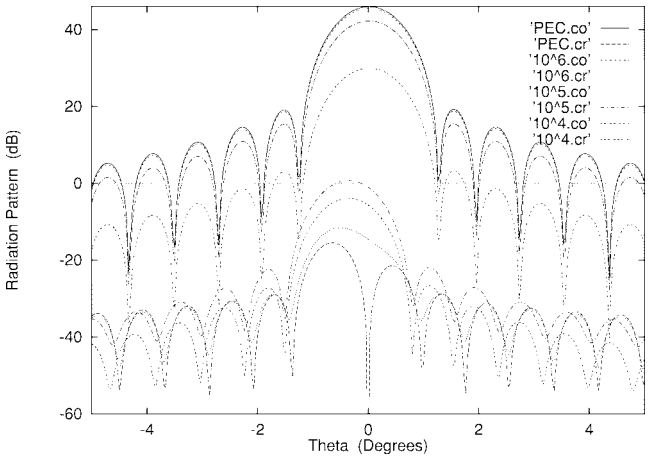

Fig. 15. Far-field radiation patterns in the $\phi = 90^\circ$ plane of the inflatable reflector antenna with different conductivities (S/m) of metal. The antenna is a 15-m offset-parabolic reflector fabricated of mylar backed by aluminum on the reflective surface and indium tin oxide on the radome surface. The frequency is 1.4 GHz (L-band).

tion on the performance of the direct-broadcast TV reflector antenna systems and the effects of finite thickness and finite conductivity on the performance of a representative inflatable antenna were presented. Results of analysis and engineering characteristizations of the two antenna systems were detailed. In general, both the electric and magnetic currents are required. However, if the antenna surface is thin or the conductivity of the reflector surface is high, application of the electric current may be sufficient. Though only single-reflector antenna systems were studied, the analysis can be applied to multiple reflector antennas as well.

APPENDIX A
PLANE WAVE PROPAGATION THROUGH PLANAR, MULTILAYERED STRUCTURES: THE TRANSMISSION LINE ANALOGY

For any oblique incidence, the rays can be resolved into two components—one parallel and one perpendicular to the interface. Consider the cases of perpendicular E-field polarization of each of the ray components. The ray component parallel to the interface is physically a TEM wave traveling along that interface (Fig. 16). The ray component perpendicular to the interface is a TEM wave which produces a standing wave pattern in the z direction due to the multiple reflections internal to the multilayered structure (Fig. 16). If we consider the cases of parallel E-field polarization of the ray components instead, we arrive at exactly the same conclusion (Fig. 16).

Since the modal voltages and currents of a TEM wave system are well-defined, the transmission line analogy can be applied. As the two components are not independent, solving one will automatically solve for the other. Hence, it will be sufficient to work entirely on the ray component perpendicular to the interface (z component), where the equivalent transmission line analogy can be used.

Two cases of oblique incidence are possible, namely, the parallel and perpendicular polarizations. We will consider them separately.

A. Perpendicular Polarization

Since the z component of any incident plane wave regardless of its polarization is essentially TEM wave at normal incidence, the transmission line analogy can be applied. A transmission line is completely characterized if its characteristic impedance and propagation constant are specified.

To evaluate the equivalent impedance of the z component of the ray we notice that

$$E_y = Ee^{-\gamma \cos\theta z} \tag{59}$$

$$H_x = -H\cos\theta e^{-\gamma\cos\theta z} \tag{60}$$

$$\Rightarrow Z = \frac{-E_y}{H_x} = \frac{E}{H\cos\theta} = \eta\ \sec\theta \tag{61}$$

where $\eta = \sqrt{\frac{\mu}{\epsilon}}$ is the intrinsic impedance of the medium. Note that the square root may be complex since both μ and ϵ can be complex in case of lossy system.

The equivalent propagation constant is just the z component of the propagation constant

$$\gamma_z = \gamma\cos\theta \tag{62}$$

where

$$\gamma = \alpha + j\beta = j\omega\sqrt{\mu\epsilon} \tag{63}$$

α and β are the attentuation and phase constants, respectively. Note that the square root may again be complex since both μ and ϵ can be complex in case of lossy system. Thus, the propagation constant and characteristic impedance of the equivalent transmission line model of the above medium are $\gamma\cos\theta$ and $\eta\sec\theta$, respectively.

Now consider the situation of oblique incidence on a multilayered system (Fig. 17). For oblique incidence, the transmission lines representing different media can be cascaded as in Fig. 18, where i and t are the indexes to the semi-unbounded incident and transmitted media, respectively. The sine and cosine of θ_1, θ_2, $\cdots$, θ_n can be obtained according to Snell's Law of Refraction [12, p. 210]

$$\gamma_j \sin\theta_j = \gamma_k \sin\theta_k \tag{64}$$

$$\Rightarrow \sin\theta_k = \frac{\gamma_j}{\gamma_k}\sin\theta_j \tag{65}$$

$$\cos\theta_k = \sqrt{1-\sin^2\theta_k} \tag{66}$$

for $j,k = 1,2,\cdots,n,i,t$.

Note that θ, $\sin\theta$, and $\cos\theta$ can be complex. The sign of the square root is chosen such that the wave is propagating and attenuating in $+z$ direction, i.e.,

$$\mathrm{Re}(\gamma_k\cos\theta_k) \geq 0 \tag{67}$$

$$\mathrm{Im}(\gamma_k\cos\theta_k) \geq 0. \tag{68}$$

By writing $V = E_y$, $I = -H_x$, the cascaded transmission-line system can be represented by the cascaded matrices mathematically [22, pp. 39–45]

$$\begin{bmatrix} V_i \\ I_i \end{bmatrix} = \begin{bmatrix} A_1 & B_1 \\ C_1 & D_1 \end{bmatrix}\begin{bmatrix} A_2 & B_2 \\ C_2 & D_2 \end{bmatrix}\cdots\begin{bmatrix} A_n & B_n \\ C_n & D_n \end{bmatrix}\begin{bmatrix} V_t \\ I_t \end{bmatrix} \tag{69}$$

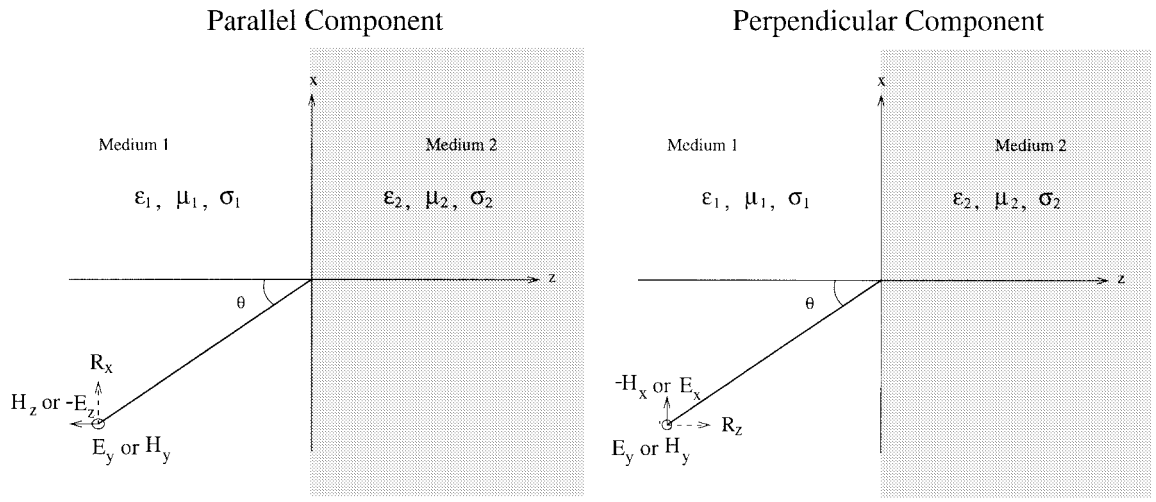

Fig. 16. Ray components parallel and perpendicular to the interface: perpendicular E-field polarization [(E_y, H_z) for the perpendicular component and $(E_y, -H_x)$ for the parallel component] and parallel E-field polarization [$(H_y, -E_z)$ for the perpendicular component and (H_y, E_x) for the parallel component].

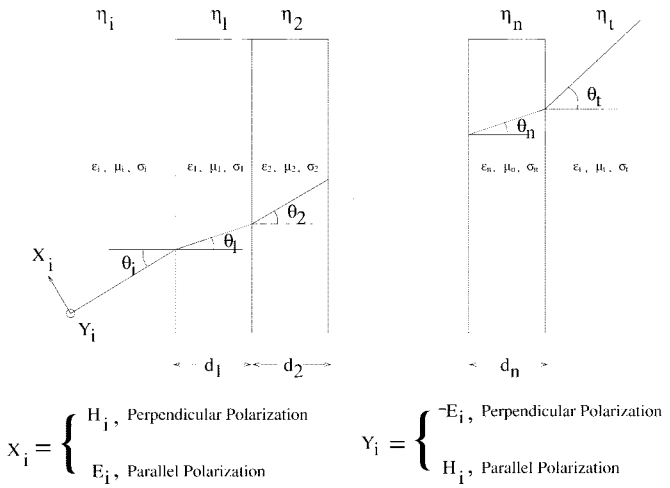

Fig. 17. Propagation of waves through multilayered media: perpendicular and parallel E-field polarizations.

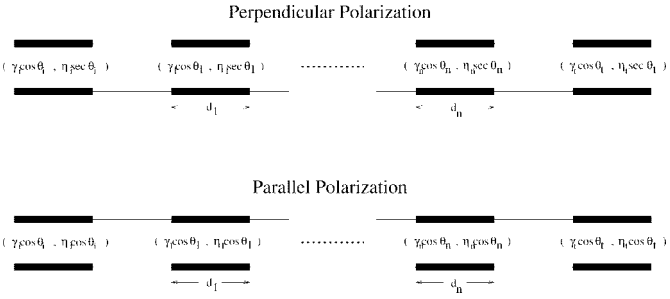

Fig. 18. Equivalent transmission lines for multilayered system at oblique incidence: perpendicular and parallel E-field polarizations.

where

$$A_m = \cosh(\gamma_m \cos\theta_m d_m) \tag{70}$$

$$B_m = \sinh(\gamma_m \cos\theta_m d_m) Z_m \tag{71}$$

$$C_m = \frac{\sinh(\gamma_m \cos\theta_m d_m)}{Z_m} \tag{72}$$

$$D_m = \cosh(\gamma_m \cos\theta_m d_m) \tag{73}$$

for $m = 1, 2, \cdots, n$. Note that V_i, I_i are the incidence voltage and current immediately before entering medium 1, and V_t, I_t are those immediately after exiting medium n. Thus, the overall reflection coefficient $(\Gamma_\perp)$ at the first interface and transmission coefficient $(\tau_\perp)$ at the last interface can be expressed as follows:

$$V_i = E_i(1 + \Gamma_\perp) \tag{74}$$

$$I_i = \frac{E_i(1 - \Gamma_\perp)}{Z_i} \tag{75}$$

where

$$Z_i = \eta_i \sec\theta_i, \quad Z_t = \eta_t \sec\theta_t. \tag{76}$$

Let

$$\begin{bmatrix} A & B \\ C & D \end{bmatrix} = \begin{bmatrix} A_1 & B_1 \\ C_1 & D_1 \end{bmatrix} \begin{bmatrix} A_2 & B_2 \\ C_2 & D_2 \end{bmatrix} \cdots \begin{bmatrix} A_n & B_n \\ C_n & D_n \end{bmatrix}. \tag{77}$$

Solving for $\Gamma_\perp$ and $\tau_\perp$ we have

$$\Gamma_\perp = \frac{A + \frac{B}{Z_t} - Z_i\left(C + \frac{D}{Z_t}\right)}{A + \frac{B}{Z_t} + Z_i\left(C + \frac{D}{Z_t}\right)} \tag{78}$$

$$\tau_\perp = \frac{2}{A + \frac{B}{Z_t} + Z_i\left(C + \frac{D}{Z_t}\right)}. \tag{79}$$

B. Parallel Polarization

The situation for parallel polarization is very much the same as that of perpendicular polarization. To find the equivalent impedence of the z component of the ray, we observe that

$$E_x = E\cos\theta e^{-\gamma\cos\theta z} \tag{80}$$

$$H_y = H e^{-\gamma\cos\theta z} \tag{81}$$

$$\Rightarrow Z = \frac{E_x}{H_y} = \frac{E\cos\theta}{H} = \eta\ \cos\theta. \tag{82}$$

Again, the equivalent propagation constant is just the z component of the the propagation constant

$$\gamma_z = \gamma\cos\theta \tag{83}$$

where

$$\gamma = \alpha + j\beta = j\omega\sqrt{\mu\epsilon} \tag{84}$$

Thus, the propagation constant and characteristic impedance of the equivalent transmission line model of the above medium are $\gamma\cos\theta$ and $\eta\ \cos\theta$, respectively.

Now consider the situation of oblique incidence on a multilayered system (Fig. 17). For oblique incidence, the transmission lines representing different media can be cascaded as in Fig. 18. The sine and cosine of θ_1, θ_2, $\cdots$, θ_n can be obtained in exactly the same way as those for the perpendicular polarization—according to the Snell's law of refraction.

By writing $V = E_x$, $I = H_y$, the cascaded transmission-line system can be represented by the same cascaded matrices as discussed previously. The overall reflection coefficient $(\Gamma_{\|})$ and transmission coefficient $(\tau_{\|})$ at the first interface can be expressed as follows:

$$V_i = E_i(1+\Gamma_{\|}) \tag{85}$$

$$I_i = \frac{E_i(1-\Gamma_{\|})}{Z_i} \tag{86}$$

where

$$Z_i = \eta_i\cos\theta_i, \quad Z_t = \eta_t\cos\theta_t. \tag{87}$$

Solving for Γ and τ, we come to the results similar to those derived in Section V-A1

$$\Gamma_{\|} = \frac{A+\frac{B}{Z_t}-Z_i\left(C+\frac{D}{Z_t}\right)}{A+\frac{B}{Z_t}+Z_i\left(C+\frac{D}{Z_t}\right)} \tag{88}$$

$$\tau_{\|} = \frac{2}{A+\frac{B}{Z_t}+Z_i\left(C+\frac{D}{Z_t}\right)}. \tag{89}$$

Hence, the same transmission lines for perpendicular incidence can be used except that the impedances changed from $\sec\theta_m$ to $\cos\theta_m$ for $m = 1,2,\cdots,n,i,t$.

REFERENCES

[1] Y. Rahmat-Samii, "Recent advances in diffraction analysis of reflector antennas," in *Directions in Electromagnetic Wave Modeling, Proceedings of the International Conference*, H. L. Bertoni and L. B. Felsen, Eds. New York: Plenum, 1991, pp. 39–65.

[2] D.-W. Duan and Y. Rahmat-Samii, "A generalized diffraction synthesis technique for high-performance reflector antennas," *IEEE Trans. Antennas Propagat.*, vol. 43, pp. 27–40, Jan. 1995.

[3] Y. Rahmat-Samii, "Reflector antennas," in *Antenna Hanbook*, Y.-T. Lo and S.-W. Lee, Eds. New York: Van Nostrand Reinhold, 1993, vol. II, pp. 15:1–124.

[4] A. G. Roederer and Y. Rahmat-Samii, "Unfurlable satellite antennas: A review," *Ann. Telecommun.*, vol. 44, nos. 9/10, pp. 475–488, Sept./Oct. 1989.

[5] Y. Rahmat-Samii and S.-W. Lee, "Vector diffraction analysis of reflector antennas with mesh surfaces," *IEEE Trans. Antennas Propagat.*, vol. AP-33, pp. 76–90, Jan. 1985.

[6] W. A. Imbriale, V. Galindo-Israel, and Y. Rahmat-Samii, "On the reflectivity of complex mesh surfaces (spacecraft reflector antennas)," *IEEE Trans. Antennas Propagat.*, vol. 39, pp. 1352–1365, Sept. 1991.

[7] Y. Rahmat-Samii and A. N. Tulintseff, "Diffraction analysis of frequency selective reflector antennas," *IEEE Trans. Antennas Propagat.*, vol. 41, pp. 476–487, Apr. 1993.

[8] M. Thomas, "Inflatable space structures," *IEEE Potentials*, vol. 11, no. 4, pp. 29–32, Dec. 1992.

[9] L. C. Schroeder, M. C. Bailey, R. F. Harrington, B. M. Kendall, and T. G. Campbell, "Design studies of large aperture, high-resolution earth science microwave radiometers compatible with small launch," NASA Tech. Paper 3469, Nat. Tech. Inform. Serv., Sept. 1994.

[10] K.-W. Lo and T. S. Bird, "Effect of dielectric coatings on parabolic reflector antenna performance," *Microwave Opt. Technol. Lett.*, vol. 8, no. 1, pp. 1–4, Jan. 1995.

[11] M. Shimba, T. Sato, and H. Koike, "The antenna pattern degradation by snow accretion on the reflector surface," in *IEEE Antennas Propagat. Soc. Int. Symp.*, Syracuse Univ., Syracuse, NY, June 1988, vol. 2, pp. 871–874.

[12] C. A. Balanis, *Advanced Engineering Electromagnetics*. New York: Wiley, 1989.

[13] D.-W. Duan and Y. Rahmat-Samii, "Novel coordinate system and rotation transformations for antenna applications," *Electromagn.*, vol. 15, no. 1, pp. 17–40, Jan./Feb. 1995.

[14] P. Ramanujam, L. F. Lopez, C. Shin, and T. J. Chwalek, "A shaped reflector design for the 'Direct TV' direct-broadcast satellite for the United States," in *IEEE Antennas Propagat. Soc. Int. Symp.*, Ann Arbor, MI, June 28–July 2, 1993, pp. 788–791.

[15] D.-W. Duan and Y. Rahmat-Samii, "Beam squint determination in conic-section reflector antennas with circularly polarized feeds," *IEEE Trans. Antennas Propagat.*, vol. 39, pp. 612–619, May 1991.

[16] T. Battilana, "Ensure uniformity when specifying paint for reflectors: A novel technique provides precise measurements of reflector coatings without need of sophisticated equipment," *Microwaves Radio Frequencies*, vol. 27, no. 3, pp. 113–122, Mar. 1988.

[17] T. Y. Otoshi, "Maximum and minimum return losses from a passive two-port network terminated with a mismatched load," *IEEE Trans. Microwave Theory Tech.*, vol. 42, pp. 787–792, May 1994.

[18] B. M. Kendall, M. C. Bailey, L. C. Schroeder, and R. F. Harrington, "Inflatable antenna microwave radiometer for soil moisture measurement," in *2nd Topical Symp. Combined Opt.-Microwave Earth Atmosph. Sensing*, Atlanta, GA, Apr. 1995, pp. 217–219.

[19] D. Lodgard, P. Ashton, M. Cho, T. Codiana, R. Geith, S. Mayeda, K. Nagel, and S. Sze, "ISAAC: Inflatable satellite of an antenna array for communications, final report 1987–88," NASA Contractor Rep., NASA CR-184704, California State Polytechnic Univ., Aerosp. Eng. Dept., Pomona, CA, 1988, vol. 6.

[20] G. S. Hickey and T.-K. Wu, "A four-frequency selective surface spacecraft subreflector antenna," *Microwave J.*, vol. 39, no. 5, pp. 240–252, May 1996.

[21] T. Gerfin and M. Gratzel, "Optical properties of tin-doped indium oxide determined by spectroscopic ellipsometry," *J. Appl. Phys.*, vol. 79, no. 3, pp. 1722–1729, Feb. 1996.

[22] A. Ishimaru, *Electromagnetic Wave Propagation, Radiation, and Scattering*. Englewood Cliffs, NJ: Prentice Hall, 1991.

Hung-Piu Ip was born in Hong Kong. He received the B.S. degree in electrical engineering from the National Taiwan University, Taipei, Taiwan, in 1992, and the M.S. degree in electrical engineering from the University of California, Los Angeles, (UCLA) in 1997.

From 1992 to 1994, he was a Computer System Hardware Design Engineer in Taiwan. From 1994 to 1997 he was employed by the UCLA Electrical Engineering Department as a Teaching and Research Assistant. His research topics include wave propagation in complex multilayered media, high-frequency asymptotic techniques, and reflector antennas design and analysis. He is currently a Radio Frequency Wireless Design Engineer, working on cellular and radio frequency and antenna circuit systems.

Yahya Rahmat-Samii (S'73–M'75–SM'79–F'85), for a photograph and biography, see p. 748 of the June 1998 issue of this TRANSACTIONS.